

CAAP Quarterly Report

Date of Report: April 10th 2019

Prepared for: *U.S. DOT Pipeline and Hazardous Materials Safety Administration*

Contract Number: 693JK31850008CAAP

Project Title: Fluorescent Chemical Sensor Array for Detecting and Locating Pipeline Internal Corrosive Environment

Prepared by: Dr. Ying Huang and Dr. Wenfang Sun

Contact Information: Dr. Ying Huang, Email: ying.huang@ndsu.edu, Phone: 701.231.7651

For quarterly period ending: April 7th 2019

Business and Activity Section

(a) Contract Activity

Discussion about contract modifications or proposed modifications

None.

Discussion about materials purchased

None.

(b) Status Update of Past Quarter Activities

In this quarter, the university research team worked on Task 2.1 and Task 2.2 of the above mentioned project, including successfully development of color change based sensors to detect CO_3^{2-} , S^{2-} , F^{3+} , and pH changes, respectively, and numerical analysis on the srurvibility of possible installation of the polymer based sensors inside the pipeline, in addition to an outreach program to low-income minority elementary and middle school students on every Thursday afternoon for eight weeks to expand the educational impact of this project.

(c) Cost share activity

Tuition Waiver for two graduate students (9 credits per student, \$693.68 per credit) ended up with \$12,486 of cost share in this quarter).

(d) Task 2: Development of Fluorescent/Colorimetric Chemical Sensor Array for Internal Corrosive Water Detection

In this quarter, two subtasks were focused on including Task 2.1 (Development of Fluorescent/Colorimetric Chemical Sensor Array) and Task 2.2 (Calibration of The Fluorescent/colorimetric Chemical Sensor Array). The detail findings are described as below:

1. Background and Objectives in the 2st Quarter

1.1 Background

This project is designed to develop passive colorimetric/fluorescent chemical sensor array for locating and detecting corrosive water inside pipes. Inside the pipelines, the transported crude oil may include a hot mixture of free water, carbon dioxide (CO₂), hydrogen sulfide (H₂S) and microorganisms. The different chemical components inside oil/water environment such as HCO₃⁻ / CO₃²⁻, Fe³⁺, S²⁻, H⁺ or pH may result in different internal corrosion mechanisms, such as sweet corrosion or sour corrosion. The passive colorimetric sensor array to be developed in this project is intended to detect the concentration changes of the five above mentioned important chemical species in the internal oil/water environment of the pipeline and use these detected environmental data to predict the internal corrosion progressing of pipelines.

1.2 Objectives in the 2nd Quarter

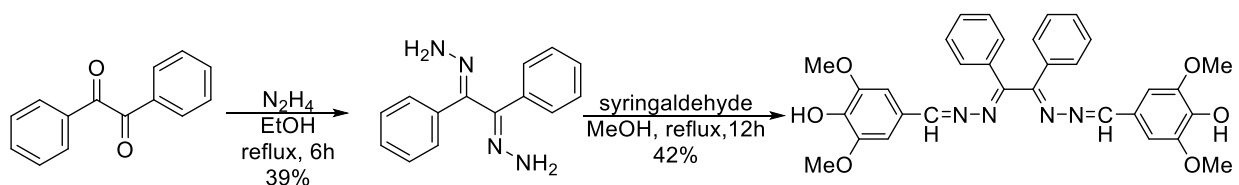
In this quarter, we have 1) successfully synthesized four sensor compounds and tested their sensing ability toward CO₃²⁻, S²⁻, Fe³⁺, and pH values, respectively. The color change and emission color or intensity changes upon addition of the analytes were studied in solutions and on the surface of filter paper to test the sensitivity of the sensing molecules in solution and on solid substrate; 2) numerically analyzed the survivability of installing the polymer sensors inside the pipe in the condition when cleaning pigs passing; and 3) performed a series of outreach events to low-income minority elementary and middle school students to expand the educational impacts.

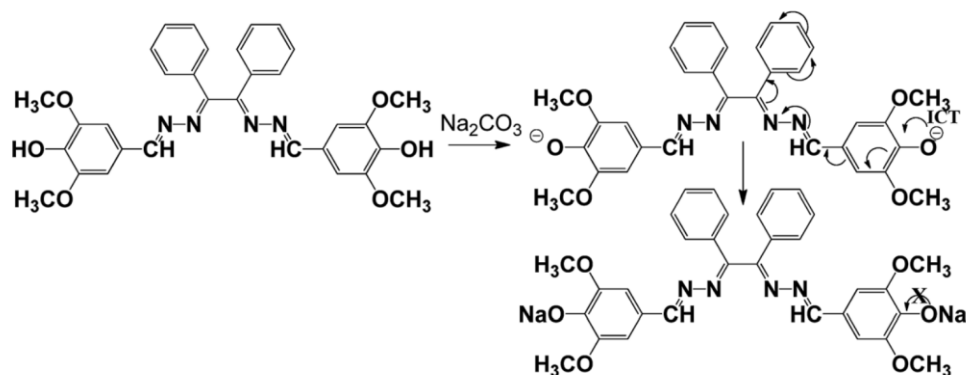
2. Results and Discussions

2.1 Development of Fluorescent/Colorimetric Chemical Sensor Array (Task 2.1)

The results below show the successfully synthesized sensor compounds and their sensing ability toward CO₃²⁻, S²⁻, Fe³⁺, and pH values, respectively.

2.1.1 Colorimetric Chemical Sensor for Detecting CO₃²⁻: For CO₃²⁻ sensing, we synthesized **sensor molecule 1** (structure shown in Scheme 3) and tested its color change and emission color/intensity changes upon addition of CO₃²⁻ ions. As shown in Figure 1, upon addition of CO₃²⁻ ions to the ethanol solution of **sensor molecule 1**, the solution color changed drastically from yellow to orange (Figure 1). On the filter paper, the color changed from pale yellow to bright yellow. Quantitative measurement showed that a new absorption band started to appear at 460 nm upon adding 50 μM CO₃²⁻ ions (Figure 2). This band kept increasing when the concentration of the CO₃²⁻ ions increased. The drastic color change should be attributed to the deprotonation of the OH group on the sensor molecule, which changed the phenol structure in the molecule to the quinone form and changed the N-N single bond to the N=N diazo bond. However, the emission color/intensity change was too weak to be visualized either in solution or on the filter paper substrate.





Scheme 1. Structure, synthetic route, and the sensing mechanism for the CO_3^{2-} anion sensor **1**.

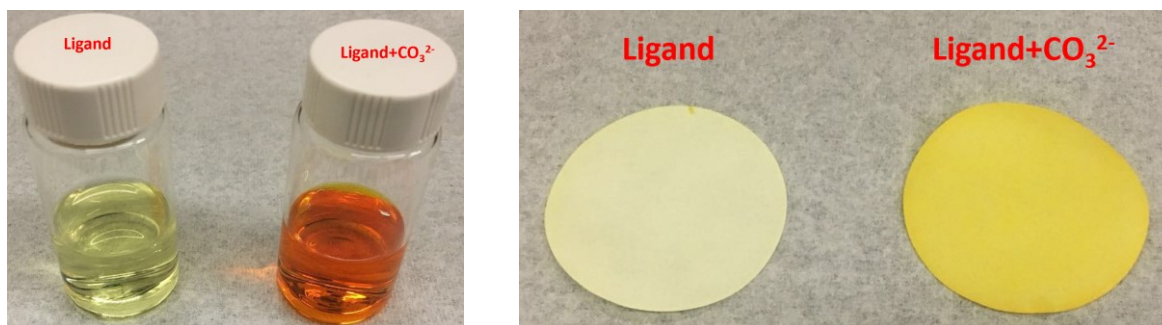


Figure 1. Photographs of the color change in EtOH solutions and on the filter paper substrates for the CO_3^{2-} sensor **1**.

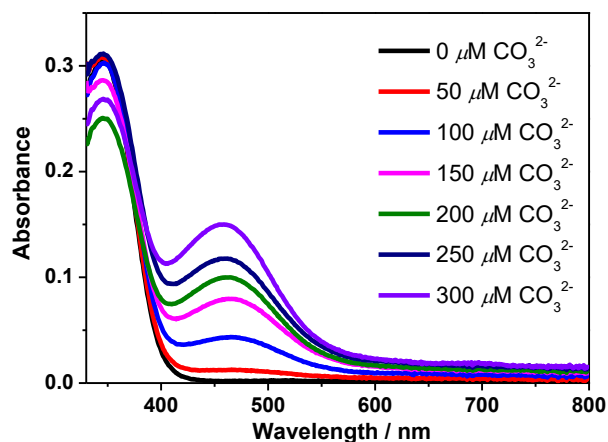
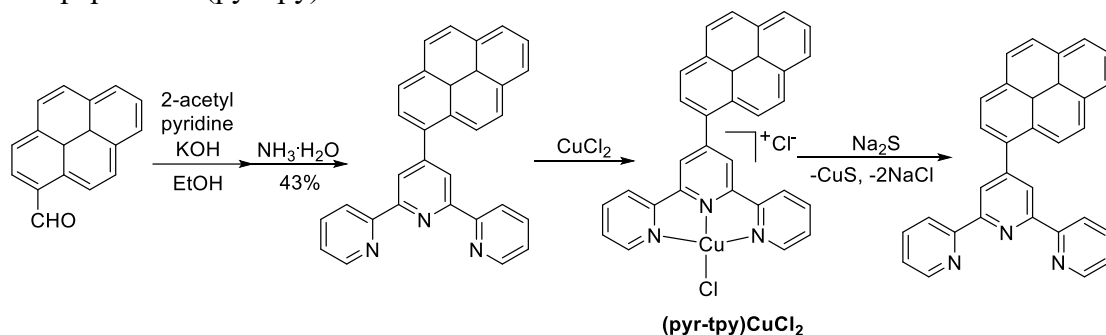


Figure 2. Quantitative measurement of the absorption change of **sensor molecule 1** in EtOH (100 μM) upon addition of different concentrations of CO_3^{2-} .

2.1.2 Fluorescent Chemical Sensor for Detecting S^{2-} : For S^{2-} sensing, we synthesized one pyrenyl-substituted terpyridine (pyr-tpy) and coordinated it to Cu^{2+} to form the Cu(II) complex (pyr-tpy) CuCl_2 as **sensor molecule 2**. This complex has a pale yellow color and is nonemissive (see the left bottles and filter papers in panels a-d in Figure 3). Upon addition of S^{2-} , the coordinated Cu^{2+} was abstracted to form the CuS precipitates, which made the solution cloudy and showed the dark color (the dark color should arise from the CuS precipitates). Meanwhile, the fluorescence from the ligand (i.e. pyr-tpy) was restored, which showed a bright blue emission (see the right bottle in panel b and the right filter paper in panel d). The quantitative emission measurement upon addition of S^{2-} anion demonstrated that the fluorescence of pyr-tpy was switched on upon addition of 50 μM S^{2-} (Figure 4). With the increased concentration of S^{2-} anion, the emission intensity kept increasing until the S^{2-} concentration reached 125 μM , at which point the

emission reached the maximum intensity. The switch on of the emission can be observed both in solution and on the filter paper with (pyr-tpy)CuCl₂ adsorbed.



Scheme 2. Structure, synthetic route and sensing mechanism of **sensor molecule 2** for the S²⁻ anion sensor (pyr-tpy)CuCl₂.

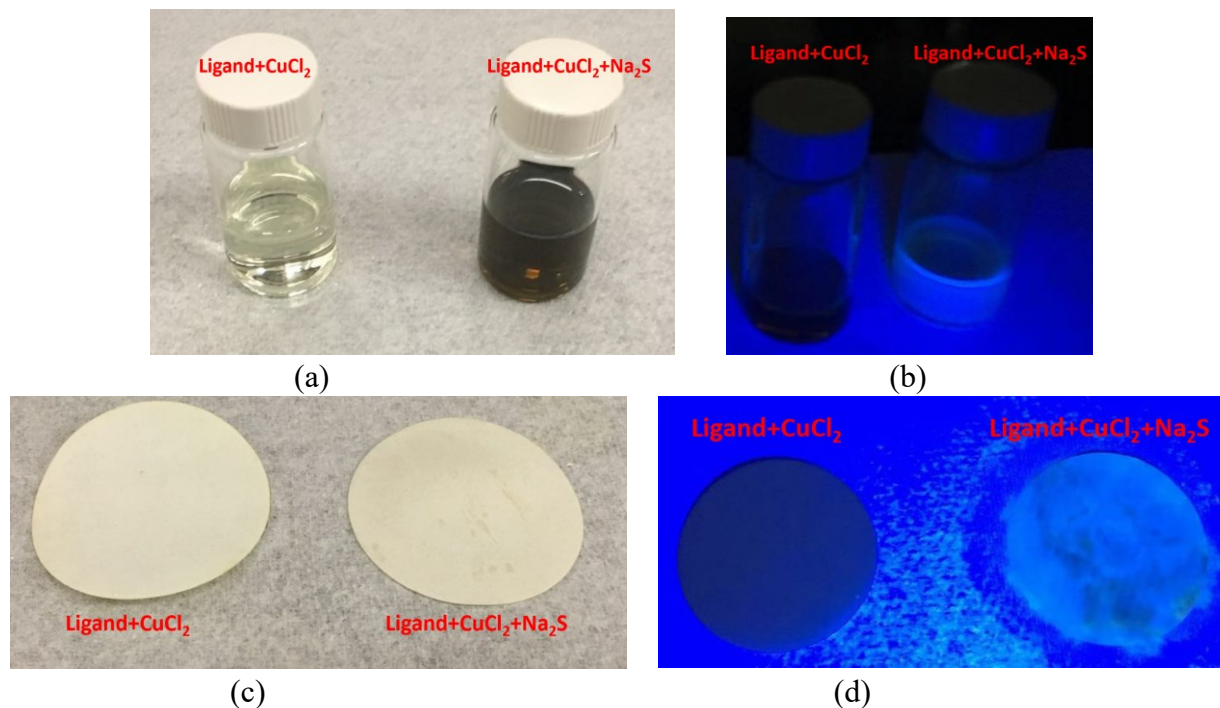


Figure 3. Photographs of the color change (panels a and c) and fluorescence switch-on (panels b and d) in solutions and on the filter paper substrates for the S²⁻ sensor (pyr-tpy)CuCl₂. The excitation wavelength for observing the fluorescence switch-on was 365 nm.

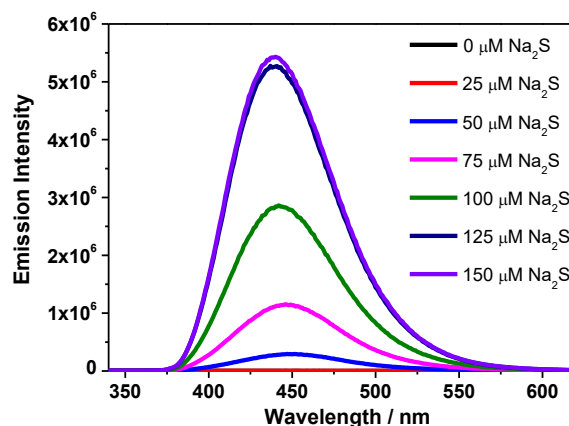
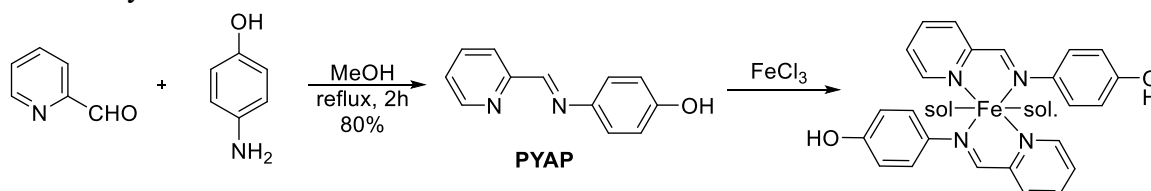


Figure 4. Quantitative measurement of the fluorescence switch-on of (pyr-tpy)CuCl₂ of **sensor molecule 2** in EtOH (100 μM) upon addition of different concentrations of Na₂S. λ_{ex} = 320 nm.

2.1.3 Colorimetric Chemical Sensor for Detecting Fe^{3+} : For Fe^{3+} sensing, we synthesized the compound **PYAP** (structure shown in **Scheme 3**) and studied its color and emission color/intensity changes upon addition of Fe^{3+} ions in solution and on the filter paper substrate as shown in Figure 5. **PYAP** showed a yellow color with very weak blue emission. Upon addition of Fe^{3+} ions, the color of the **PYAP** EtOH solution changed to purple blue both in solution and on the filter paper. Quantitative measurement of addition of different concentrations of Fe^{3+} ions to the EtOH solution of **PYAP** caused a significant blue-shift of the major absorption band accompanied by the appearance of a new band at ca. 490 nm (Figure 6a). Meanwhile, a new emission band appeared at ca. 590 nm (Figure 6b). The changes in the absorption and emission spectra occurred upon addition of 50 μM Fe^{3+} ion. However, the changes in emission color and intensity was unable to be visualized either in solution or on the filter paper because of the very weak emission intensity.



Scheme 3. Structure, synthetic route and sensing mechanism for the Fe^{3+} cation sensor **PYAP**.

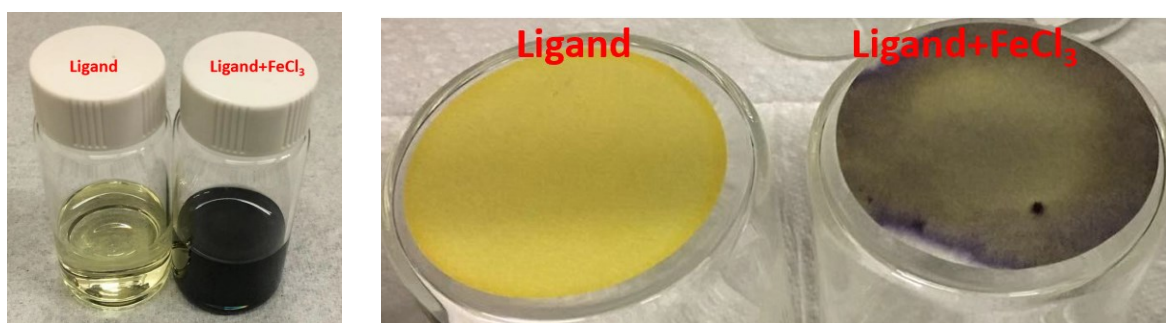


Figure 5. Photographs of the color change in EtOH solutions and on the filter paper substrates for the Fe^{3+} sensor **PYAP**.

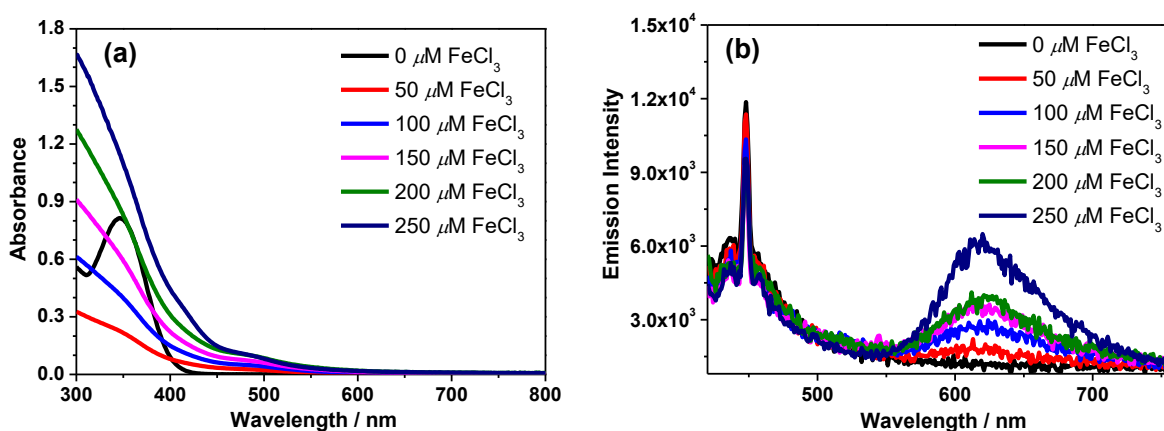
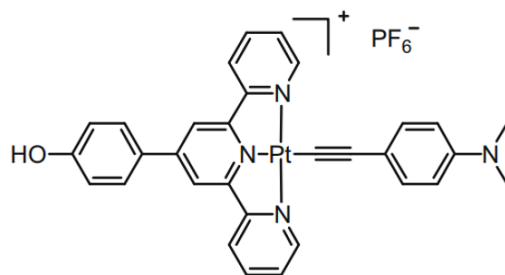


Figure 6. Quantitative measurement of the absorption change and fluorescence switch-on of **PYAP** in EtOH (200 μM) upon addition of different concentrations of $FeCl_3$. $\lambda_{ex} = 395$ nm.

2.1.4 Colorimetric Chemical Sensor for Detecting H^+ and pH: We have tested the pH responses of one of our Pt(II) complexes as **Scheme 4** in CH_3CN solutions and on filter paper substrates at different pH values. As shown in Figure 7, the original color of the complex was purple at pH = 7. At pH = 3, the color changed to yellow due to the protonation of the $-N(CH_3)_2$ group. Under basic condition (pH = 11), the color changed

to blue, due to deprotonation of the OH group. Figure 8 shows the quantitative measurement of the UV-vis absorption spectral changes of the complex at different pH values. Acidic condition caused a drastic blue-shift of the absorption spectrum, while basic conditions caused the red-shift of the absorption spectrum.



Scheme 4. Structure of the Pt(II) complex as a pH sensor.



Figure 7. Photographs of the color change in CH_3CN solutions and on the filter paper substrates for the Pt(II) complex as a pH sensor.

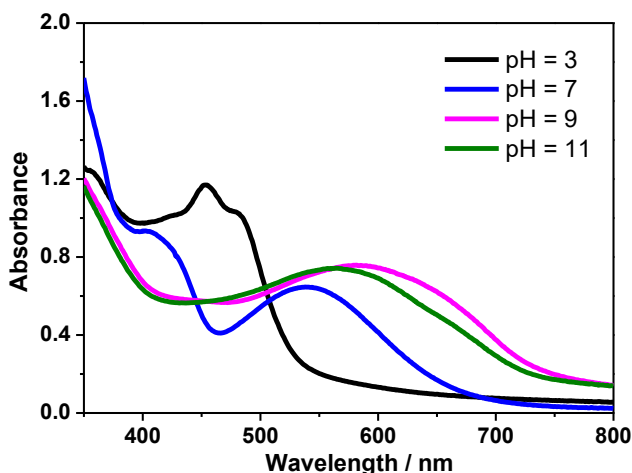


Figure 8. Quantitative measurement of the absorption spectrum change of the Pt(II) complex in CH_3CN ($100 \mu\text{M}$) at different pH values.

2.2 Calibration of The Fluorescent/colorimetric Chemical Sensor Array (Task 2.2)

The sections below show the numerical analysis results on the sensitivity study on the survivability of the polymer sensors inside the pipe in the condition when cleaning pigs passing.

2.2.1 Sensor Array Survivability in Oil/Water Environment: Before widely deployed, survivability of sensor arrays is an essential issue for an expected service period. When the oil/gas products are being transported, sever heat, pressure and speed are applied to reach the demand for flow rate. All these destructive external conditions pose a huge challenge to the survivability of the sensors. In addition, the regular cleaning behavior by introducing Pipeline Investigation Gauges also demands the sensors for resisting against pressure and hard scratch. Pigging is now a standard procedure in petroleum and natural gas industry. Fluid or gas is pumped upstream to provide necessary force for cleaning the wax and sediments or dewatering.

The traveling portion of a typical PIG is made up of a rigid and hollow center body and two sets of sealing discs. Clamp plates are used to hold each sealing disc in place on either side of the main rigid body. The PIG with sealing discs made of polyurethane rubber is usually propelled down the line due to the flow in the pipeline. According to this procedure, in this quarter, a 2-dimensional axisymmetric finite element model (FEM) was employed to analyze the internal stress of sensors when a sealing disc passes. The profile of the model is shown in Figure 9 and Table 1 shows the detail parameters used in this numerical analysis. The inner diameter of the steel pipe was assumed to be 324mm with a thickness of 8mm. Regular A36 steel was used as steel pipe material in the analysis. The disk on the cleaning pigs, also known as sealing disk, was assumed to have a thickness of 15mm and a diameter of 340 mm, which is 5% oversized when compared with the inner diameter of the pipe. The material of the sealing disk was assumed to be rubber. On the cleaning pigs, clamping plates are usually made by steel to fix the sealing disks into proper space. In this analysis, as seen in Table 1, the thickness of the clamp plates was assumed to be 15mm with an outer diameter of 200mm. In this model, the clamping plates were moving forward from the left along the x-axis as seen in Figure 9, forcing the sealing disk to move with them.

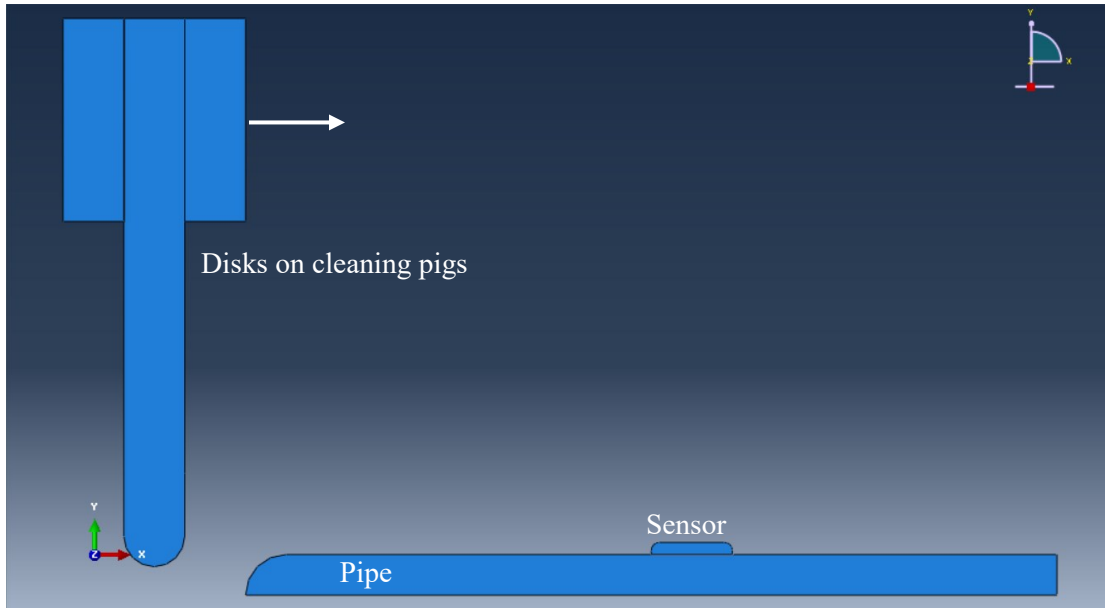


Figure 9. FEM Model sketch.

Table 1. FEM model dimension details.

Pipe inner diameter(mm)	Pipe thickness(mm)	Clamp plates thickness(mm)	Clamp plates outer diameter(mm)	Sealing disk thickness(mm)	Sealing disk outer diameter(mm)
324	8	15	200	15	340 (5% oversized)

In FEMs, the material of the sealing disk, rubber, is always considered as hyperelastic, which indicates high elasticity, ductility, and deformation restoring after unloading. Thus, the Mooney-Rivlin model, a hyperelastic material model, is used to simulate this material. In the Mooney-Rivlin model, the strain energy density, W , is a linear combination of two invariants of the left Cauchy-Green deformation tensor as shown in Equation 1. The detail material properties of the sealing disk used in the analysis are listed in Table 2.

$$W = C_1(I_1 - 3) + C_2(I_2 - 3) \quad (1)$$

in which, C_1 , C_2 are the empirically determined material constants, and I_1, I_2 are the first and second

invariant of Cauchy-Green deformation tensor.

Table 2. Material properties of rubber (the sealing disk).

Density	Poisson's Ratio	Hardness (Shore A)	C ₁₀	C ₀₁
1350kg/m ³	0.35	85	1.926	0.963

For the sensor, epoxy was assumed as the polymer matrix to dope the chemical sensors, due to its high density, good mechanical properties, water resistance, and impermeability. The material parameters of the epoxy (sensor) used in the analysis are listed in Table 3.

Table 3. Material properties of epoxy (the sensor).

Density(kg/m ³)	Elastic Modulus (MPa)	Tensile Modulus (MPa)	Flexural Modulus (MPa)	Shear Modulus (MPa)
1540	1000	10500	10000	1250

2.2.2 Sensitivity Study: To investigate the sensitivity of the sensor thickness on the sensor and the cleaning disk, sensors of different thickness varies from 1 to 10 mm were analyzed to study the optimal design to avoid excessive internal stress and failure the for survivability of sensor array. A sequence of steps of the deformation when the sealing disk passed the sensor is shown in Figure 10 and the maximum stress in the sensor and sealing disk is listed in Table 4 and Figure 11.

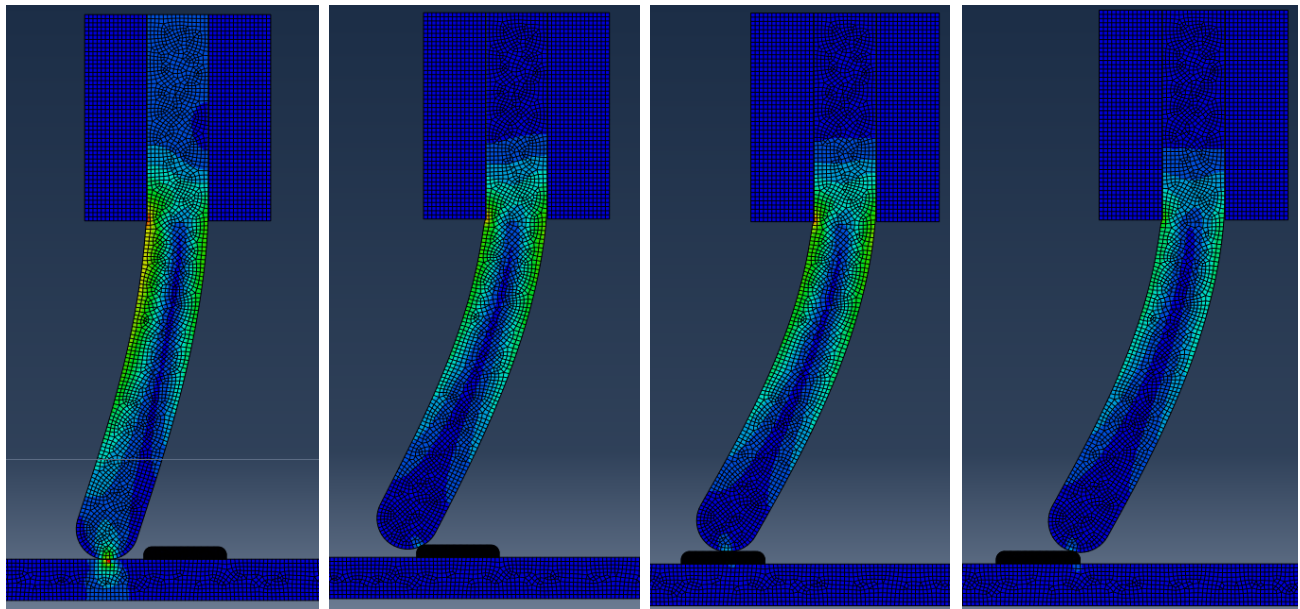


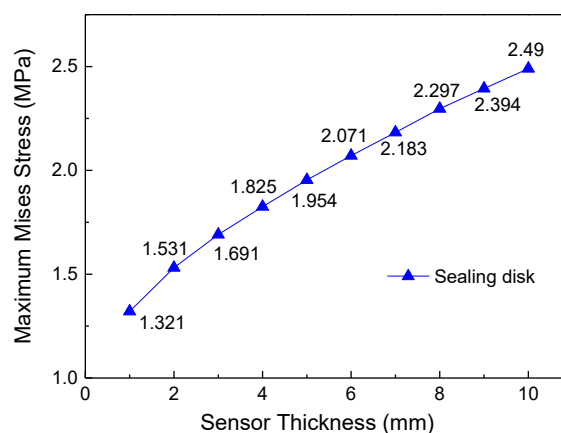
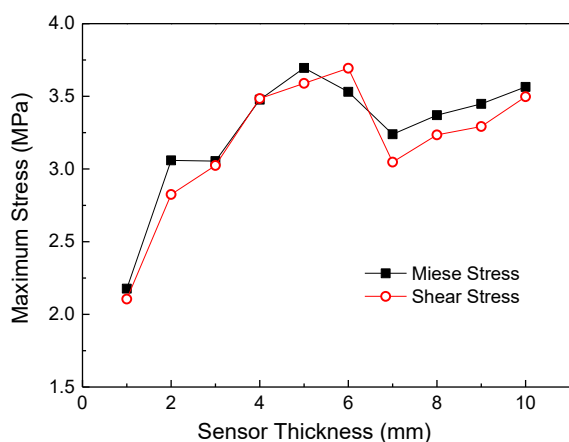
Figure 10. Deformation simulation results.

As illustrated in Figure 10, the process of the sealing disk passing the sensor can be divided into four stages: (1) start-up stage, (2) climbing stage, (3) scratch stage and (4) decline stage. In the first stage, the sealing disk began to come in contact with the sensor, the bending angle of the disk and contact stress began to increase. In the second stage, the bending angle and stress in the sensor increased sharply to a certain value, this is when maximum stress happened in the sensor. In the following stage, the sealing disk scratched the top surface of the sensor. The inner stress of the sensor remained relatively stable but less than the maximum stress experienced. In contrast, the stress of the sealing disk remained peaked during this progress. In the last stage, the sensor was unloaded due to the detachment from the sealing disk which reset to contact with the pipe.

Results as shown in Figure 11 and Figure 12 indicate that the increase of sensor thickness leads to a continuous increase of stress in both sensors and sealing disks. Furthermore, for sensors less than 3mm in thickness, the maximum internal stress remained less than or slightly exceeded 3MPa, and 3mm to 10mm thickness would cause an obvious growth in Mises stress (over 3MPa), which contributes to material failure by distortion. Thus, if epoxy is the polymer material selected to dope the chemical sensors, the thickness less than 3 mm would be the most recommended because of the lower level of stress (less than 3MPa). For the sealing disk, when passing through the sensor base, it presented the same stress level as in the sensor. Regarding the field application and good mechanical properties of polyurethane, which is the common material used in sealing disks, the stress in it should be considered secondly compare to the sensor. If a material different than epoxy is selected in next quarter to dope the sensor molecules, the FEM models will be updated to reflect that changes on the sensor size design.

Table 4. Maximum stress of sensors with different thickness.

Sensor thickness(mm)	Maximum Mises Stress of sensor (Mpa)	Maximum Shear Stress of sensor (Mpa)	Maximum Mises Stress of bending portion in sealing disk(MPa)
1	2.177	2.105	1.321
2	3.059	2.825	1.531
3	3.054	3.024	1.691
4	3.477	3.485	1.825
5	3.695	3.589	1.954
6	3.531	3.693	2.071
7	3.239	3.047	2.183
8	3.370	3.235	2.297
9	3.448	3.292	2.394
10	3.565	3.497	2.490



(a) Maximum stress of sensor base

(b) Maximum stress of sealing disk

Figure 11. Maximum stress of the sensors in different thickness

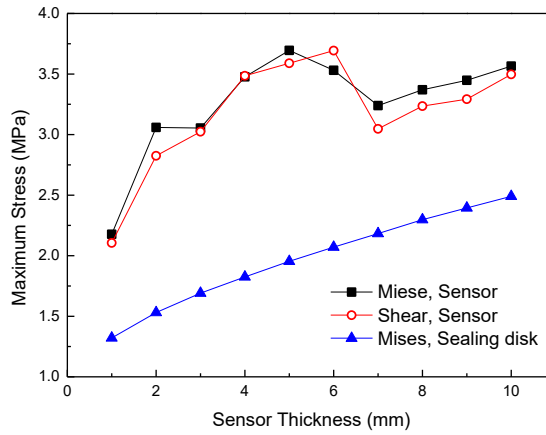


Figure 12. Maximum stress of the sensors in different thickness

2.3 Student Advising and Outreach

2.3.1 Student Advising: During the first quarter, three graduate students (Wei Xu, Ph.D. student, Shuomang Shi, Ph. D. student, and Hafiz Usman Ahmed, masters student) and two new undergraduate research assistants (Erika Krieger and Kaitlin Hennen) were hired to work on this project. The three graduate students worked on this project during Quarter 2 and they will continue work on this project next quarter. The two undergraduate students were hired from Jan 2019 to May 2019. In the summer, no undergraduate research assistant will work on this project, the two research assistants will come back in August 2019 to continue working on this project.

2.3.2 Outreach Activities: In this quarter, the PI started a new outreach program to promote corrosion related transportation and water resources engineering to minority young generations. It offers an seven-week workshop at four different centers as shown in Table 5 on every Thursday afternoon to underserved youth, including low-income families, refugees, and young girls. Table 6 shows the scheduled dates for each outreach event performed in the past quarter, the activities were performed from 3pm to 5:30pm each Thursday as indicated in the dates. This outreach program closely works with “CHARISM” (a neighborhood support center for low-income families) and “Society of Women Engineer” (SWE, a society to promote STEM to young girls). All the civil engineering undergraduate and graduate assistants in this project participated this outreach program, including Kaitlin Hennen (junior), Erika Krieger (junior), Shuomang Shi (Ph. D. student), Hafiz Usman Ahmed (Masters), and Xinyi Yang (Masters). Figure 13 show several photos taken during the outreach events. It turned out to be a very successful outreach program.

Table 5. Center locations

Center Name	Number of Kids	Grade
Carl Ben	20	Middle school
Ed Clapp	22	Elementary school
Lewis and Clark	22	Elementary school
McCormick	35	Elementary school

Table 6. Scheduled outreach event dates

Dates (3pm to 5:30pm)
Feb 14 2019
Feb 21 2019
March 07 2019
March 21 2019
March 28 2019

April 04 2019

April 11 2019



Figure 13. Photos of the outreach events

3. Future work

In the third quarter, there will be three objectives:

- 1) Task 2.1: Find an appropriate polymer matrix to dope the chemical sensor molecules for coating thin films on the steel substrate;
- 2) Task 2.2: Update FEM models based on the polymer selection in Task 2.1 and perform parametric analysis using FEM analysis on sensor aspect ratio, multiple pig velocity, and material selection would be considered to advise the sensor casting;
- 3) Task 2.2: Survivability of the sensors in oil/gas environments with flow considered;
- 4) Student Advising and Outreach: Continue advising graduate and undergraduate students and continue performing the outreach events.